# Microscopic analysis of the ground state properties of the even-even Dy isotopes in the reflection-asymmetric relativistic mean-field theory

Yu-Ting Qiu, Xiao-Wei Wang, and Jian-You Guo [*]

*School of Physics and Optoelectronics Engineering, Anhui University, Hefei 230601, People's Republic of China*

Reflection-asymmetric relativistic mean-field theory is used to explore the ground state properties for the even-even Dy isotopes. The results are compared with those from the finite-range droplet model (FRDM), the deformed relativistic Hartree-Bogoliubov theory in continuum (DRHBc), and the available data. The calculated binding energies and quadrupole deformations agree with the experimental data as well as the FRDM and DRHBc calculations. The obtained matter density distributions and potential energy surfaces clearly exhibit the ground state shapes and the presence of deformation in these nuclei. The experimental fingerprints of octupolarity in $^{148,154,156,160}$Dy around $N = 88$ are convincing in the present calculations. The predictions on the octupole deformation in $^{190-194,200,202}$Dy around $N = 134$ agree with the results from the FRDM calculations. In addition, we obtain more knowledge about the shape evolution and phase transition from oblate to pear shape and then to prolate shapes in the Dy isotopes.

## I. INTRODUCTION

The shape evolution and phase transition is an interesting topic in nuclear physics, which has revealed abundant insight into microscopic details of nuclear structure. As we know, the ground states of most medium-mass and heavy nuclei are reflection symmetric and display spherical or ellipsoidal shapes. However, there are also some nuclei whose shapes break the reflection symmetry. This phenomenon was detected experimentally as early as the 1950s. The Berkeley group observed low excited states of negative parity in actinides [1–3], which means that the nuclei can spontaneously break their spatial reflection symmetry and acquire nonzero octupole moments associated with reflection-asymmetric shapes (pear shapes) [4–6]. Microscopically, strong octupole correlations can be attributed to the coupling between the adjacent single-particle states with $\Delta l = \Delta j = 3$ near the Fermi surface [7]. The most important octupole coupling occurs between the single-particle energy levels $1g_{9/2} \leftrightarrow 2p_{3/2}$, $1h_{11/2} \leftrightarrow 2d_{5/2}$, $1i_{13/2} \leftrightarrow 2f_{7/2}$, and $1j_{15/2} \leftrightarrow 2g_{9/2}$, corresponding to proton (neutron) numbers 34, 56, 88, and 134 [8,9].

The search for the octupole-deformed nuclei in the nuclear chart is one of the important frontiers in the study of nuclear structure. Theoretical and experimental explorations on the octupole-deformed nuclei mainly focus on the neutron-rich lanthanides around $Z = 56$ and $N = 88$ and light actinides around $Z = 88$ and $N = 134$. Recently, the octupolarity in $^{220}$Rn and $^{224}$Ra was investigated by the Coulomb excitation experiments, and the measured $E3$ strength shows that there is strong octupole deformation in $^{224}$Ra [10], which is the first experimental evidence of static octupole-deformed even-even nucleus. Similar experiments were performed to explore the octupole deformation in $^{144}$Ba [11] and $^{146}$Ba [12], and the available data confirm the presence of octupole deformation in the region centered on the neutron-rich Ba isotopes. The observations of low-lying states in $^{224}$Rn and $^{226}$Rn [13] show that radon isotopes undergo octupole vibrations but do not have static reflection-symmetric shapes in their ground states. Fingerprints of stable pear shapes are also found in $^{222,228}$Ra and $^{228}$Th [14,15]. In order to explore the octupole-deformed nuclei and understand their exotic properties, many theoretical methods with the degrees of freedom of octupole deformation have been applied to investigate the ground state properties of atomic nuclei, such as the macroscopic-microscopic model [16–18], the self-consistent mean-field method [19–22], the interaction boson model [23–27], the reflection-asymmetric shell model [28], the generator coordinate method [29–33], the quadrupole-octupole collective Hamiltonian [34–36], and microscopic calculations based on the energy density functionals [37,38].

The relativistic mean-field (RMF) theory is one of the most successful microscopic models and is widely used in the study of ground state properties [39–43]. Recently, this theory has been used to explore the octupole-deformed nuclei [44–48] including the shape evolution and phase transition [49,50] and shape coexistence [51]. To include conveniently the reflection-asymmetric degrees of freedom, Geng *et al.* have established the reflection-asymmetric relativistic mean-field (RASRMF) theory [52]. Based on the RASRMF theory, they have investigated the ground state properties for the octupole-deformed nucleus $^{226}$Ra and well reproduced the experimental data. Zhang *et al.* have applied the RASRMF to investigate the octupole deformation for the Sm and Ba

_____
[*]Corresponding author: jianyou@ahu.edu.cn

isotopes and demonstrated their shape evolution and phase transition features [53,54]. In Refs. [55,56], we have applied the RASRMF to investigate the shape evolution for the even-even Th and Ce isotopes and found that the degrees of freedom of octupole deformation play an important role in the ground state properties of these nuclei.

In order to extensively study the octupole deformation in atomic nuclei, Cao *et al.* have performed a systematic survey of ground state shapes for the even-even nuclei with $Z \leqslant 110$ and $N \leqslant 210$ by the nuclear density functional theory [37]. Besides the traditional octupole-deformation regions ($Z \approx 88$ and $N \approx 134$, and $Z \approx 56$ and $N \approx 88$), they have found that there are the reflection-asymmetric deformations in the neutron-rich nuclei around $^{200}$Gd.

Recently, the octupole deformation in the Dy isotopes have received additional attention. Much effort has been devoted to exploring octupole deformation in the Dy isotopes. The spectroscopy of low-spin states in $^{157}$Dy is studied in Ref. [57], where the observed interlacing band structures are interpreted as the bands of parity doublets with simplex quantum number $s = -i$ related to possible octupole correlations. The octupole vibrations in $^{152}$Dy [58], the $E1$ transitions in $^{154}$Dy [59], and the negative-parity band structure in $^{162}$Dy [60] and $^{156}$Dy [61] have been observed experimentally, which stimulates the interest in exploring the octupole correlations in the Dy isotopes. Usmanov *et al.* have analyzed the mixing of octupole vibrational bands in $^{160}$Dy with a phenomenological model [62]. The ground state and low-energy negative-parity bands of $^{156}$Dy have been studied in Ref. [63] and the experimental data [61] have been reproduced well. Zhao *et al.* investigated the ground state properties for $^{160,162,164}$Dy. The available potential energy surfaces show that these nuclei are $\beta_3$ soft, and the energy minimum lies in the direction of axial octupole deformation $\beta_3$ [64].

To better understand the octupole deformation in the Dy isotopes, we apply the RASRMF theory to systematically study the ground state properties for the Dy isotopes. The calculated binding energies and deformations have reproduced the experimental data. The available matter density distributions and potential energy surfaces show that the reflection-asymmetric degrees of freedom play an important role in the ground state properties of atomic nuclei. In addition to these nuclei discovered experimentally, we have also explored the nuclei far from the stability line and obtained more knowledge on the shape evolution and phase transition in the Dy isotopes. Furthermore, the predictive power of the RASRMF theory is convincing in comparison with the experimental data and the finite-range droplet model (FRDM) and deformed relativistic Hartree-Bogoliubov theory in continuum (DRHBc) calculations. This paper is organized as follows. The RASRMF theory is sketched in Sec. II. The numerical details and results are presented in Sec. III. A summary is given in Sec. IV.

## II. FORMALISM

To explore the novel properties for the nuclei with reflection-asymmetric degrees of freedom, we first present the theoretical formalism. The starting point of the relativistic

mean-field theory is an effective Lagrangian density [39–42]:

$$
\begin{aligned}
\mathcal{L} = &\bar{\psi}[i\gamma^\mu \partial_\mu - M - g_\sigma \sigma - g_\omega \omega_\mu \gamma^\mu - g_\rho \vec{\rho}_\mu \vec{\tau} \gamma^\mu \\
&- \tfrac{1}{2}e\gamma^\mu(1 - \tau_3)A_\mu]\psi + \tfrac{1}{2}(\partial_\mu \sigma \partial^\mu \sigma - m_\sigma^2 \sigma^2) \\
&- \tfrac{1}{4}\omega^{\mu\nu}\omega_{\mu\nu} + \tfrac{1}{2}m_\omega^2 \omega^\mu \omega_\mu - \tfrac{1}{3}g_2 \sigma^3 - \tfrac{1}{4}g_3 \sigma^4 \\
&- \tfrac{1}{4}\vec{\rho}^{\mu\nu}\vec{\rho}_{\mu\nu} + \tfrac{1}{2}m_\rho^2 \vec{\rho}^\mu \vec{\rho}_\mu + \tfrac{1}{4}c_3(\omega^\mu \omega_\mu)^2 \\
&- \tfrac{1}{4}A^{\mu\nu}A_{\mu\nu},
\end{aligned}
\tag{1}
$$

where $\psi$ is the Dirac spinor of the nucleon with the corresponding mass $M$, $\sigma$ is the isoscalar-scalar meson that provides medium-range attraction, $\omega$ is the isoscalar-vector meson that provides short-range repulsion, $\rho$ is the isovector-vector meson reflecting the difference of neutron and proton, and $A$ is the photon field describing the electromagnetic properties of atomic nuclei.

Starting from the Lagrangian density, with the classical variational principle, the Dirac equation for the nucleons,

$$
\{-i\vec{\alpha} \cdot \vec{\nabla} + V(\vec{r}) + \beta[M + S(\vec{r})]\}\psi_i = \epsilon_i \psi_i, \tag{2}
$$

and the Klein-Gordon equations for the mesons,

$$
\begin{aligned}
[-\Delta + m_\sigma^2]\sigma(\vec{r}) &= -g_\sigma \rho_s(\vec{r}) - g_2 \sigma^2(\vec{r}) - g_3 \sigma^3(\vec{r}), \\
[-\Delta + m_\omega^2]\omega^\mu(\vec{r}) &= g_\omega j^\mu(\vec{r}) - g_4(\omega^\nu \omega_\nu)\omega^\mu(\vec{r}), \\
[-\Delta + m_\rho^2]\rho^\mu(\vec{r}) &= g_\rho \vec{j}^\mu(\vec{r}), \\
-\Delta A^\mu(\vec{r}) &= e j_\rho^\mu(\vec{r}),
\end{aligned}
\tag{3}
$$

are obtained. Equations (2) and (3) are nonlinear coupled equations, which are very difficult to be solved strictly. In order to easily obtain the solutions of Eqs. (2) and (3), the basis expansion method is often used. For the axially symmetric deformed nuclei, the Dirac spinors can be presented as

$$
\begin{pmatrix} f_i(r, s, t) \\ ig_i(r, s, t) \end{pmatrix} = = \frac{1}{\sqrt{2\pi}}
\begin{pmatrix}
f_i^+(z, r_\perp)e^{i(\Omega_i - \frac{1}{2})\varphi} \\
f_i^-(z, r_\perp)e^{i(\Omega_i + \frac{1}{2})\varphi} \\
ig_i^+(z, r_\perp)e^{i(\Omega_i - \frac{1}{2})\varphi} \\
ig_i^-(z, r_\perp)e^{i(\Omega_i + \frac{1}{2})\varphi}
\end{pmatrix} x_{t_i}(t), \tag{4}
$$

where $\Omega_i$ is the third component of angular momentum. To include the reflection-asymmetric degrees of freedom, the eigenfunctions of the two-center harmonic-oscillator (TCHO) potential are used as the basis to expand the Dirac spinors $f_i^\pm$ and $g_i^\pm$ in the RMF calculations. The TCHO potential [52] has the following form:

$$
V(r_\perp, z) = \frac{1}{2}M\omega_\perp^2 r_\perp^2 +
\begin{cases}
\frac{1}{2}M\omega_1^2(z + z_1)^2, & z < 0, \\
\frac{1}{2}M\omega_2^2(z - z_2)^2, & z \geqslant 0.
\end{cases}
\tag{5}
$$

Here, $z_1$ and $z_2$ represent the distance from the center of the ellipsoid to the plane of their intersection, and $\omega_1$ ($\omega_2$) corresponds to the oscillation frequency of the harmonic oscillator for $z < 0$ ($z \geqslant 0$), respectively.

The TCHO potential can be completely determined by the following three parameters: $\delta_2$, $\delta_3$, and $\Delta z$. $\delta_2$ is the quadrupole deformation parameter in the hemisphere with $z > 0$. $\delta_3$ is the asymmetric coefficient of TCHO, $\delta_3 = \omega_1/\omega_2$. When $\delta_3 = 1$, the system is axially symmetric. $\Delta z(= \Delta z_1 + \Delta z_2)$ represents the center distance of the TCHO basis. Here,

we mainly focus on the reflection-asymmetric deformation and do not discuss the effect of $\Delta z$ in the properties. Therefore, the value of $\Delta z$ in the calculation is consistent with Ref. [52].

In order to obtain the potential energy surfaces, i.e., the total binding energy as a function of deformation, we perform the constrained RMF calculations. The binding energies under different shapes ($\beta_2$, $\beta_3$) can be obtained by constraining the quadrupole moment $\langle \hat{Q}_2 \rangle$ and the octupole moment $\langle \hat{Q}_3 \rangle$ to given values $\mu_2$ and $\mu_3$ [65] simultaneously, i.e.,

$$\langle H' \rangle = \langle H \rangle + \tfrac{1}{2}C_2(\langle \hat{Q}_2 \rangle - \mu_2)^2 + \tfrac{1}{2}C_3(\langle \hat{Q}_3 \rangle - \mu_3)^2, \quad (6)$$

where $C_1$ and $C_2$ are two spring constants, and $\mu_2$ and $\mu_3$ are the given quadrupole and octupole moments. $\langle \hat{Q}_2 \rangle$ and $\langle \hat{Q}_3 \rangle$ are the expectation values of the quadrupole and octupole moment operators, which are expressed as $\langle \hat{Q}_2 \rangle = \langle 2r^2 P_2(\cos\theta) \rangle$ and $\langle \hat{Q}_3 \rangle = \langle 2r^3 P_3(\cos\theta) \rangle$, respectively. The deformation parameter $\beta_2$ is related to $\langle \hat{Q}_2 \rangle$ by $\langle \hat{Q}_2 \rangle = \frac{3}{\sqrt{5\pi}}AR^2\beta_2$ with $R = r_0 A^{\frac{1}{3}}$ ($r_0 = 1.2$ fm) and $A$ is the mass number. Similarly, the relationship between the deformation parameter $\beta_3$ and the moment $\langle \hat{Q}_3 \rangle$ is $\langle \hat{Q}_3 \rangle = \frac{3}{\sqrt{7\pi}}AR^3\beta_3$.

We also fix the center of mass of the nuclei at the origin under the constraints of the monopole moment operator $\langle \hat{Q}_1 \rangle$ to avoid spurious motions of the center of mass:

$$\langle \hat{Q}_1 \rangle = 0. \quad (7)$$

### III. NUMERICAL DETAILS AND RESULTS

We apply the constrained RASRMF theory to explore the novel properties for the Dy isotopes. Without loss of generality, the parameter set NL3* [66] is adopted in the present calculations. Seventeen main shells are used in the TCHO basis, the convergence of the numerical calculations is checked. The pairing correlations are treated with the BCS approximation by fixing the energy gap $\Delta = 11.2/A^{1/2}$ MeV. The calculated binding energies are shown in Fig. 1. For convenience in comparison, the figure also shows the results from the FRDM calculations [67], the results from the DRHBc calculations [68], and the available data [69]. For the three models, the calculated binding energies are consistent with the experimental data for the Dy isotopes with mass number $A = 138–176$. Although the FDRM calculation is more in line with the experiment, the deviation of the DRHBc and the RASRMF calculations from the experimental data is also very small. The largest difference between the present calculations and the experiment data $\Delta E$ is smaller than 0.025 MeV, which appears in $^{174}$Dy. Compared with the DRHBc calculation, the RASRMF calculation matches the experiment better.

For the Dy isotopes with mass number $A = 178–208$, which have not been found in the experiment, the RASRMF calculation is more consistent with the result from the FRDM calculation, especially on the extremely neutron-rich side. In comparison with the experimental data, the extremely neutron-rich Dy isotopes predicted by the DRHBc are relatively bound. Considering that the DRHBc is only applicable to the axially symmetric deformed nuclei, this difference may reflect the importance of the reflection-asymmetric degrees of freedom.
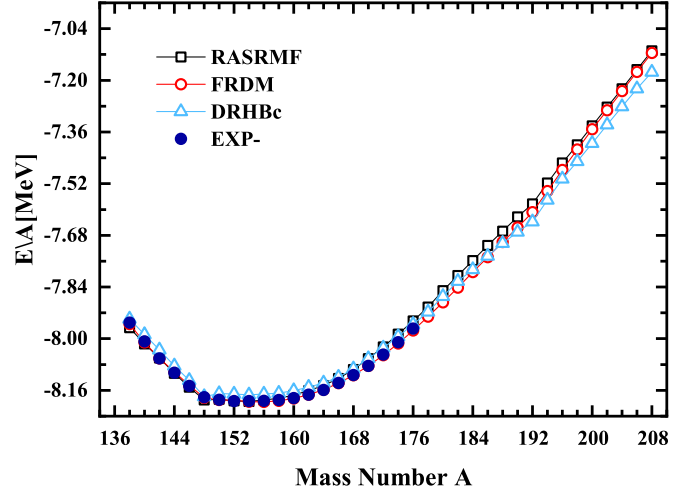


FIG. 1. The binding energy per nucleon $E/A$ and its variation with the mass number $A$ in the Dy isotopes. The results from the RASRMF calculations, the FRDM calculations, and the DRHBc calculations are denoted as open boxes, open circles, and open triangles, respectively. The experimental data are marked as closed circles.

As we know, most nuclei have axially symmetric quadrupole deformation. However, there are also some nuclei that spontaneously break their intrinsic reflection symmetry, resulting in octupole deformation in their ground states. By introducing the reflection-asymmetric degrees of freedom, the RASRMF theory can give simultaneously the quadrupole deformation $\beta_2$ and the octupole deformation $\beta_3$ of atomic nuclei.

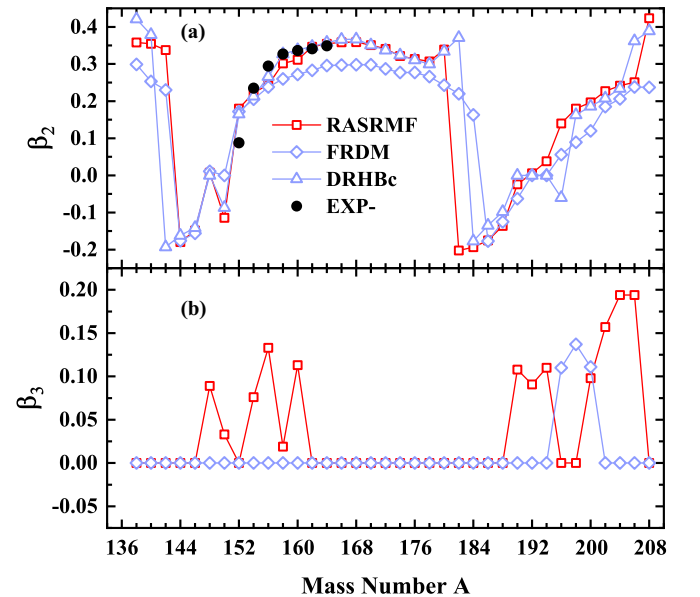The calculated deformations and their variations with mass number $A$ are shown in Fig. 2 for the Dy isotopes. That in



FIG. 2. The calculated deformations and their variations with the mass number $A$. (a) The quadrupole deformation $\beta_2$. For comparison, this figure also shows the results from the FRDM and DRHBc calculations including the available data. (b) The octupole deformation $\beta_3$ together with the results from the FRDM calculations.

Fig. 2(a) is the quadrupole deformation $\beta_2$ and its evolution to the mass number $A$, and that in Fig. 2(b) is the octupole deformation $\beta_3$ and its evolution to the mass number $A$. For comparison, the results from the FRDM and DRHBc calculations and the experimental data are also displayed there. The calculated quadrupole deformations from the RASRMF and DRHBc calculations agree better with the experimental data. There is little deviation between the FRDM calculation and experimental data, but the trend of deformation with the mass number is consistent. The largest deviation occurs in $^{158}$Dy, the difference between the calculation and the experiment $|\Delta\beta_2| = 0.067$ is small (the experimental $\beta_2 = 0.327$ and the FRDM calculated $\beta_2 = 0.26$) except $^{152}$Dy, whose quadrupole deformation is systematically overestimated in the three calculations. Over the range of the Dy isotopes considered here, the calculated quadrupole deformations are comparable in the three models. For the Dy isotopes with mass number $A = 138$–168, the calculated quadrupole deformation first decreases and then increases with the increase of mass number. The same case does appear in the Dy isotopes with mass number $A = 168$–208. For the Dy isotopes for which experimental data are not available, the $\beta_2$ values calculated by RASRMF and DRHBc are slightly larger than those calculated by FRDM. However, for the very neutron-rich region with $A > 184$, the three calculations yield similar $\beta_2$ values for most of the nuclei, up to $A = 194$ including $A = 202$ and 204. Noteworthy for these nuclei around $A = 144$, the $\beta_2$ changes rapidly from a positive value to a negative one; i.e., the shape evolves from a prolate shape to an oblate shape.

Since the DRHBc does not consider the reflection-asymmetric degrees of freedom, the Fig. 2(b) shows only the results from the RASRMF and FRDM calculations. The present calculations show that there are octupole deformations in the Dy isotopes with mass number $A = 148$, 154, 156, 160, 190–194, 200–206. While in the FRDM calculations, there is no octupole deformation in these nuclei around mass number $N = 88$, the observable octupole deformation ($|\beta_3| \geqslant 0.1$) appears in the extremely neutron-rich nuclei $^{196-200}$Dy. Considering that the experiment has given many fingerprints of octupole deformation in the Dy isotopes around $N = 88$, the theoretical predictions of RASRMF about the octupole-deformed nuclei should be more credible. For examples, the alternating parity rotation bands in $^{157}$Dy [57], the octupole vibrations in $^{152}$Dy [58], the $E1$ transitions in $^{154}$Dy [59], and the negative-parity band structure in $^{162}$Dy [60] and $^{156}$Dy [61] have been observed experimentally. These indicate there are the octupole-deformed nuclei in the Dy isotopes around $N = 88$. For the Dy isotopes around $N = 134$, although the results of these two theoretical calculations are not completely consistent, they both predict the existence of octupole-deformed nuclei.

In order to intuitively perceive the nuclear shapes and possible octupole deformations, the matter density distributions on the $x = 0$ plane as a function of $z$ and $y$ are plotted in Fig. 3. Considering that the most likely octupole-deformed nuclei locate at the two regions $N = 88$ and $N = 134$, we have only plotted the matter density distributions for the Dy isotopes with mass number $A = 146$–160 and $A = 188$–202. From Fig. 3(a), it can be seen that $^{146}$Dy is an oblate nucleus,
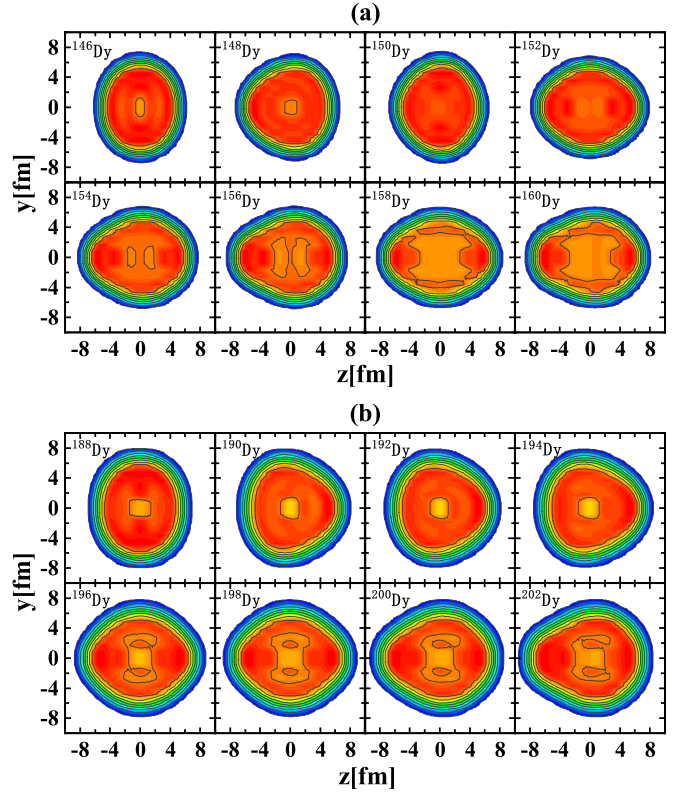


FIG. 3. The calculated matter density distributions for the ground states of Dy isotopes on the plane $x = 0$. Panel (a) is for $^{146-160}$Dy, and panel (b) is for $^{188-202}$Dy. The RASRMF calculations were performed with NL3*.

$^{148}$Dy is a pear-shaped nucleus, $^{150}$Dy is an oblate nucleus with a little octupole deformation, and $^{152}$Dy is a prolate nucleus. The matter density distributions of $^{154,156}$Dy are pear shaped, indicating that they are octupole-deformed nuclei. $^{158,160}$Dy are axially symmetric deformed nuclei. There is a little asymmetry in $^{160}$Dy. Compared with $^{148}$Dy, the octupole deformation in $^{154,156}$Dy is more significant. For the Dy isotopes from $A = 148$ to $A = 158$, there appears the shape evolution from pear to axially symmetric to pear to axially symmetric shapes, where $^{150}$Dy is a transitional nucleus from pear to axially symmetric shape, and $^{156}$Dy is a stable reflection asymmetric nucleus. As $^{150}$Dy is a transitional nucleus, it is the reason for inconsistency in the calculated deformations with RASRMF, DRHBc, and FRDM.

From Fig. 3(b), it can be seen that $^{188}$Dy is an axially symmetric oblate nucleus. There is clear octupole deformation in these $^{190-194}$Dy. Further increasing the mass number, the reflection-asymmetric deformation disappears, the nuclei $^{196,198}$Dy become a reflection-symmetric shape. Starting from $^{200}$Dy, the nuclei turn into the reflection-asymmetric shape again. Compared with $^{190-194}$Dy, the octupole deformation in $^{200,202}$Dy is more remarkable. Totally, the shape of these nuclei with $A = 188$–202 evolve from axially symmetric oblate shape to reflection-asymmetric shape, return to reflection-symmetric shape, and return to reflection-asymmetric shape again. The shape evolution is consistent with the changes of quadrupole deformation $\beta_2$ and octupole deformation $\beta_3$ shown in Fig. 2.

Although the matter density distributions clearly show the shape of these nuclei, to understand why the nucleus takes this shape, we plot the potential energy surface as the function of deformations. The contours of total binding energies as the functions of $\beta_2$ and $\beta_3$ are shown in Fig. 4 for the Dy isotopes. From Fig. 4(a), it can be seen that the energy minimum of most nuclei locates at the position $\beta_2 \neq 0$ and/or $\beta_3 \neq 0$; i.e., they are deformed nuclei. For $^{146,152,158}$Dy, the energy minimum appears in the position $\beta_3 = 0$; i.e., the ground states of these nuclei hold an axially symmetric shape. $^{146}$Dy is a fairly stable oblate nucleus because the energy minimum appears on the side $\beta_2 < 0$ and is quite deep in the potential energy surface. $^{152,158}$Dy are prolate nuclei with the energy minimum on the side $\beta_2 > 0$. Since the energy minimum of the two nuclei is considerably deep, $^{152,158}$Dy are stable prolate quadrupole-deformed nuclei. For $^{148,154,156,160}$Dy, the energy minimum appears in the position $\beta_3 \neq 0$; i.e., these nuclei hold octupole deformation. In the position of energy minimum, the quadrupole deformation $\beta_2$ in $^{148}$Dy is nearly zero; i.e., $^{148}$Dy is almost a pure octupole-deformed nucleus. Different from $^{148}$Dy, $^{154,156,160}$Dy have an octupole deformation accompanied by a large quadrupole deformation. Comparably, $^{156}$Dy is a $\beta_3$ soft nucleus since the energy minimum along $\beta_3$ extends to a large range. It is worth noting that for $^{150}$Dy, although the energy minimum appears on the oblate side, there appears an almost identical energy minimum on the prolate side; that is, $^{150}$Dy may be a coexistence nucleus of the oblate and prolate shapes, which leads to the inconsistency in the calculated deformations with RASRMF, DRHBc, and FRDM. From $^{148}$Dy to $^{158}$Dy, the potential energy surfaces clearly show the shape evolution from pear to axially symmetric to pear to axially symmetric shapes, which is consistent with the shape evolution obtained in the matter density distributions. Especially, the transitional nucleus $^{150}$Dy and remarkably reflection asymmetric nucleus $^{156}$Dy can be identified from the potential energy surface.

Similar to Fig. 4(a), Fig. 4(b) shows that the energy minimum of most nuclei locates at the position $\beta_2 \neq 0$ and/or $\beta_3 \neq 0$; that is, they are deformed nuclei. $^{188}$Dy is a quadrupole-deformed nucleus with an oblate shape for energy minimum on the side $\beta_2 < 0$. For $^{190-194}$Dy, the energy minimum appears in the position $\beta_3 \neq 0$; i.e., the ground states of these nuclei hold octupole deformation. For $^{196,198}$Dy, the energy minimum appears at the positions with $\beta_2 > 0$ and $\beta_3 = 0$ and is relatively deep in comparison with their neighbors. Namely, the ground state of these nuclei has much quadrupole deformation. Different from $^{196,198}$Dy, the energy minimum for $^{200,202}$Dy appears at the positions $\beta_2 > 0$ and $\beta_3 \neq 0$ and is quite deep in their potential energy surfaces. It indicates that $^{200,202}$Dy are considerably stable octupole-deformed nuclei. For the Dy isotopes with mass number from $A = 188$ to $202$, the potential energy surfaces show that octupole deformation happens at $^{190-194,200,202}$Dy. Compared with $^{190-194}$Dy, $^{200,202}$Dy are more stable octupole-deformed nuclei and may be detected experimentally.
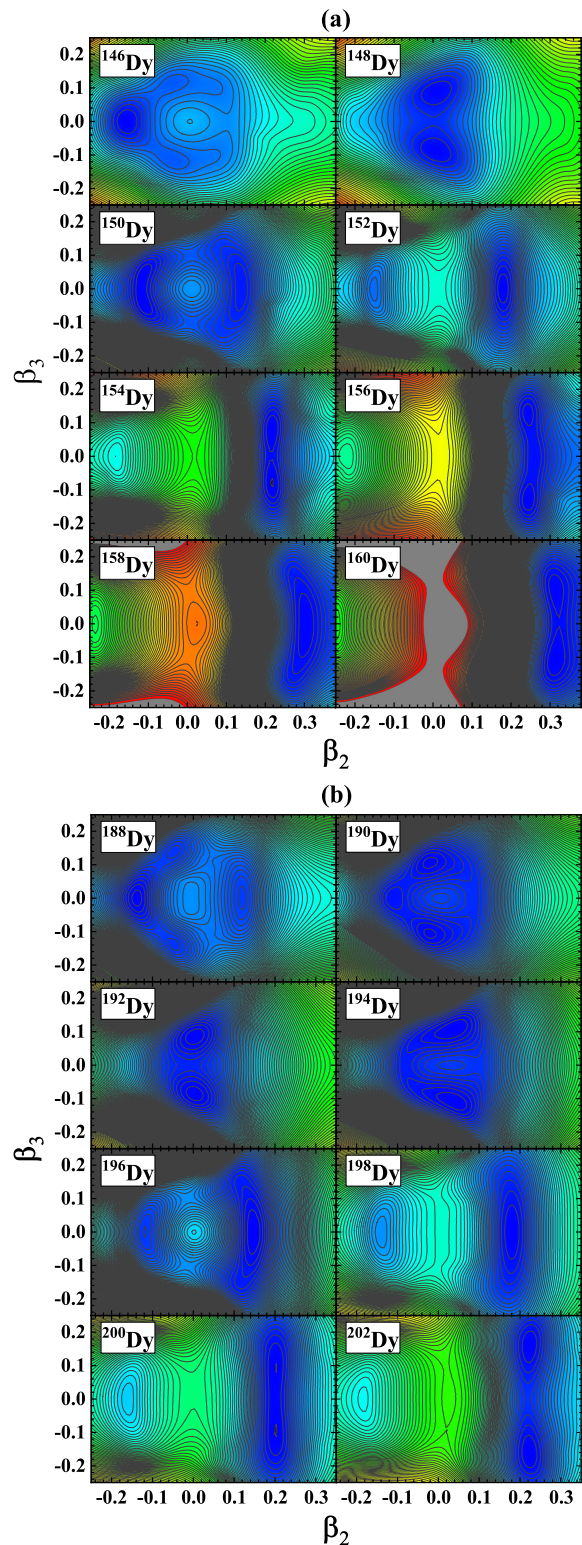


FIG. 4. The available potential energy surfaces versus the quadrupole deformation $\beta_2$ and the octupole deformation $\beta_3$ in the present calculations. Panel (a) is for $^{146-160}$Dy and panel (b) is for $^{188-202}$Dy. The RASRMF calculations are performed with NL3*.

## IV. SUMMARY

In summary, the RASRMF theory is used to explore the ground state properties for the even-even Dy isotopes. The calculated binding energies agree with the experimental data. Compared with the DRHBc calculations, the present calculations match the experiment better. In addition, that the present calculations agree better the FRDM calculations for the unknown Dy isotopes may originate from this consideration of the reflection-asymmetric degrees of freedom.

The calculated quadrupole deformations are consistent with the experimental data as well as the DRHBc calculations. There is little deviation between the FRDM calculations and experimental data, but the deformation trend is consistent. Especially, the experimental fingerprints of octupole deformation in the Dy isotopes around $N = 88$ are convincing in the present calculations. The prediction of octupole deformation in the extremely neutron-rich nuclei around $N = 132$ is in accordance with the FRDM calculations.

The available matter density distributions clearly show the ground state deformation and the shape evolution. For the Dy isotopes with $A = 146$–$160$, it is found that $^{150}$Dy is a transitional nucleus from pear to axially symmetric shape, and $^{148,154,156}$Dy are reflection-asymmetric nuclei. Compared with $^{148}$Dy, the octupole deformation in $^{154,156}$Dy is more remarkable. For the Dy isotopes with $A = 188$–$202$, there is an octupole deformation in $^{190-194}$Dy and $^{200,202}$Dy. In contrast, the octupole deformation in $^{200,202}$Dy is more significant.

The position of the ground state in the potential energy surfaces is observed with the deformations $\beta_2$ and $\beta_3$. Besides quadrupole deformation, the energy minimum of $^{148,154,156,160}$Dy locates at $\beta_3 \neq 0$, which implies they hold octupole deformation. Especially, the potential energy surfaces show $^{150}$Dy may be a coexistence nucleus of the oblate and prolate shapes and $^{156}$Dy is a stable reflection-asymmetric nucleus with a deep energy minimum of octupole deformation. Similarly, the energy minimum of $^{190-194,200,202}$Dy locates at $\beta_3 \neq 0$. From the depth of the energy minimum, it can be judged that $^{200,202}$Dy are more stable octupole-deformed nuclei.

Overall, the present calculations predict two promising regions of octupole-deformed nuclei in the Dy isotopes. One is the area near $N = 88$, including $^{148,154,156,160}$Dy, and the experimental fingerprints of octupolarity are convincing in the present calculations. The promising region is the area around $N = 134$, including $^{190-194,200,202}$Dy, which is consistent with the FRDM calculations. These are helpful for experimental exploration of octupole-deformed nuclei.

[1] F. Asaro, F. S. Stephens, and I. Perlman, Phys. Rev. **92**, 1495 (1953).

[2] F. S. Stephens, F. Asaro, and I. Perlman, Phys. Rev. **96**, 1568 (1954).

[3] F. S. Stephens, F. Asaro, and I. Perlman, Phys. Rev. **100**, 1543 (1955).

[4] V. M. Strutinsky, Physica **22**, 1166 (1956).

[5] K. Lee and D. R. Inglis, Phys. Rev. **108**, 774 (1957).

[6] S. A. Johansson, Nucl. Phys. **22**, 529 (1961).

[7] P. A. Butler, J. Phys. G: Nucl. Part. Phys. **43**, 073002 (2016).

[8] P. A. Butler and W. Nazarewicz, Rev. Mod. Phys. **68**, 349 (1996).

[9] S. C. Pancholi, Mod. Phys. Lett. A **36**, 2130013 (2021).

[10] L. P. Gaffney, P. A. Butler, M. Scheck, A. B. Hayes, F. Wenander, M. Albers, B. Bastin, C. Bauer, A. Blazhev, S. Bönig, N. Bree, J. Cederkäll, T. Chupp, D. Cline, T. E. Cocolios, T. Davinson, H. D. Witte, J. Diriken, T. Grahn, A. Herzan *et al.*, Nature (London) **497**, 199 (2013).

[11] B. Bucher, S. Zhu, C. Y. Wu, R. V. F. Janssens, D. Cline, A. B. Hayes, M. Albers, A. D. Ayangeakaa, P. A. Butler, C. M. Campbell, M. P. Carpenter, C. J. Chiara, J. A. Clark, H. L. Crawford, M. Cromaz, H. M. David, C. Dickerson, E. T. Gregor, J. Harker, C. R. Hoffman *et al.* Phys. Rev. Lett. **116**, 112503 (2016).

[12] B. Bucher, S. Zhu, C. Y. Wu, R. V. F. Janssens, R. N. Bernard, L. M. Robledo, T. R. Rodríguez, D. Cline, A. B. Hayes, A. D. Ayangeakaa, M. Q. Buckner, C. M. Campbell, M. P. Carpenter, J. A. Clark, H. L. Crawford, H. M. David, C.

Dickerson, J. Harker, C. R. Hoffman, B. P. Kay *et al.*, Phys. Rev. Lett. **118**, 152504 (2017).

[13] P. A. Butler *et al.*, Nat. Commun. **10**, 2473 (2019).

[14] P. A. Butler, L. P. Gaffney, P. Spagnoletti, K. Abrahams, M. Bowry, J. Cederkäll, G. de Angelis, H. De Witte, P. E. Garrett, A. Goldkuhle, C. Henrich, A. Illana, K. Johnston, D. T. Joss, J. M. Keatings, N. A. Kelly, M. Komorowska, J. Konki, T. Kröll, M. Lozano, B. S. Nara Singh, D. O'Donnell *et al.*, Phys. Rev. Lett. **124**, 042503 (2020).

[15] M. M. R. Chishti, D. O'Donnell, G. Battaglia, M. Bowry, D. A. Jaroszynski, B. S. N. Singh, M. Scheck, P. Spagnoletti, and J. F. Smith, Nat. Phys. **16**, 853 (2020).

[16] A. Gyurkovich, A. Sobiczewski, B. Nerlo-Pomorska, and K. Pomorski, Phys. Lett. B **105**, 95 (1981).

[17] W. Nazarewicz, P. Olanders, I. Ragnarsson, J. Dudek, G. A. Leander, P. Möller, and E. Ruchowska, Nucl. Phys. A **429**, 269 (1984).

[18] P. Möller, R. Bengtsson, B. Carlsson, P. Olivius, T. Ichikawa, H. Sagawa, and A. Iwamoto, At. Data Nucl. Data Tables **94**, 758 (2008).

[19] E. Garrote, J. L. Egido, and L. M. Robledo, Phys. Rev. Lett. **80**, 4398 (1998).

[20] L. M. Robledo and G. F. Bertsch, Phys. Rev. C **84**, 054302 (2011).

[21] S. E. Agbemava and A. V. Afanasjev, Phys. Rev. C **96**, 024301 (2017).

[22] Z. Xu and Z.-P. Li, Chin. Phys. C **41**, 124107 (2017).

[23] J. Engel and F. Iachello, Phys. Rev. Lett. **54**, 1126 (1985).

[24] D. Kusnezov and F. Iachello, Phys. Lett. B **209**, 420 (1988).

[25] K. Nomura, T. Nikšić, and D. Vretenar, Phys. Rev. C **97**, 024317 (2018).

[26] K. Nomura, R. Rodríguez-Guzmán, L. M. Robledo, J. E. García-Ramos, and N. C. Hernández, Phys. Rev. C **104**, 044324 (2021).

[27] O. Vallejos and J. Barea, Phys. Rev. C **104**, 014308 (2021).

[28] Y.-J. Chen, Z.-C. Gao, Y.-S. Chen, and Y. Tu, Phys. Rev. C **91**, 014317 (2015).

[29] J. M. Yao, E. F. Zhou, and Z. P. Li, Phys. Rev. C **92**, 041304(R) (2015).

[30] R. N. Bernard, L. M. Robledo, and T. R. Rodríguez, Phys. Rev. C **93**, 061302(R) (2016).

[31] E. F. Zhou, J. M. Yao, Z. P. Li, J. Meng, and P. Ring, Phys. Lett. B **753**, 227 (2016).

[32] P. Marević, J.-P. Ebran, E. Khan, T. Nikšić, and D. Vretenar, Phys. Rev. C **97**, 024334 (2018).

[33] Y. Fu, H. Wang, L.-J. Wang, and J. M. Yao, Phys. Rev. C **97**, 024338 (2018).

[34] Z. P. Li, B. Y. Song, J. M. Yao, D. Vretenar, and J. Meng, Phys. Lett. B **726**, 866 (2013).

[35] S. Y. Xia, H. Tao, Y. Lu, and Z. P. Li, T. Nikšić, and D. Vretenar, Phys. Rev. C **96**, 054303 (2017).

[36] K. Nomura, L. Lotina, T. Nikšić, and D. Vretenar, Phys. Rev. C **103**, 054301 (2021).

[37] Y. Cao, S. E. Agbemava, A. V. Afanasjev, W. Nazarewicz, and E. Olsen, Phys. Rev. C **102**, 024311 (2020).

[38] R. Rodríguez-Guzmán and L. M. Robledo, Phys. Rev. C **103**, 044301 (2021).

[39] B. D. Serot and J. D. Walecka, Adv. Nucl. Phys. **16**, 1 (1986).

[40] P. Ring, Prog. Part. Nucl. Phys. **37**, 193 (1996).

[41] J. Meng, H. Toki, S. G. Zhou, S. Q. Zhang, W. H. Long, and L. S. Geng, Prog. Part. Nucl. Phys. **57**, 470 (2006).

[42] J. Meng, *Relativistic Density Functional for Nuclear Structure* (World Scientific, Singapore, 2016).

[43] S. Shen, H. Liang, W. H. Long, J. Meng, and P. Ring, Prog. Part. Nucl. Phys. **109**, 103713 (2019).

[44] B.-N. Lu, J. Zhao, E.-G. Zhao, and S.-G. Zhou, Phys. Rev. C **89**, 014323 (2014).

[45] W. Zhang and Y. F. Niu, Phys. Rev. C **96**, 054308 (2017).

[46] H. Tao, J. Zhao, Z. P. Li, T. Nikšić, and D. Vretenar, Phys. Rev. C **96**, 024319 (2017).

[47] X. Meng, B.-N. Lu, and S.-G. Zhou, Sci. China Phys. Mech. Astron. **63**, 212011 (2020).

[48] K. Nomura, Phys. Rev. C **105**, 054318 (2022).

[49] K. Nomura, D. Vretenar, and B.-N. Lu, Phys. Rev. C **88**, 021303(R) (2013).

[50] K. Nomura, D. Vretenar, T. Nikšić, and B.-N. Lu, Phys. Rev. C **89**, 024312 (2014).

[51] Z. P. Li, T. Nikšić, and D. Vretenar, J. Phys. G: Nucl. Part. Phys. **43**, 024005 (2016).

[52] G. Li-Sheng, J. Meng, and H. Toki, Chin. Phys. Lett. **24**, 1865 (2007).

[53] W. Zhang, Z. P. Li, S. Q. Zhang, and J. Meng, Phys. Rev. C **81**, 034302 (2010).

[54] Z. Wei, Z. P. Li, and S. Q. Zhang, Chin. Phys. C **34**, 1094 (2010).

[55] J. Y. Guo, P. Jiao, and X.-Z. Fang, Phys. Rev. C **82**, 047301 (2010).

[56] H. Huang and J. Y. Guo, Sci. Sin. Phys. Mech. Astron. **43**, 69 (2013).

[57] S. N. T. Majola, R. A. Bark, L. Bianco, T. D. Bucher, S. P. Bvumbi, D. M. Cullen, P. E. Garrett, P. T. Greenlees, D. Hartley, J. Hirvonen, U. Jakobsson, P. M. Jones, R. Julin, S. Juutinen, S. Ketelhut, B. V. Kheswa, A. Korichi, E. A. Lawrie, P. L. Masiteng, B. Maqabuka *et al.*, Phys. Rev. C **100**, 034322 (2019).

[58] T. Lauritsen, R. V. F. Janssens, M. P. Carpenter, P. Fallon, V. B. Herskind, D. G. Jenkins, T. L. Khoo, F. G. Kondev, A. Lopez-Martens, A. O. Macchiavelli, D. Ward, K. A. Saleem, I. Ahmad, R. M. Clark, M. Cromaz, T. Døssing, A. M. Heinz, A. Korichi, G. Lane, C. J. Lister *et al.*, Phys. Rev. Lett. **89**, 282501 (2002).

[59] G. L. Zimba, J. F. Sharpey-Schafer, P. Jones, S. P. Bvumbi, L. P. Masiteng, S. N. T. Majola, T. S. Dinoko, E. A. Lawrie, J. J. Lawrie, D. Negi, P. Papka, D. Roux, O. Shirinda, J. E. Easton, and N. A. Khumalo, Phys. Rev. C **94**, 054303 (2016).

[60] A. Aprahamian, X. Wu, S. R. Lesher, D. D. Warner, W. Gelletly, H. G. Borner, F. Hoyler, K. Schreckenbach, R. F. Casten, Z. R. Shi, D. Kuznezov, M. Ibrahim, A. O. Macchiavelli, M. A. Brinkman, and J. A. Becker, Nucl. Phys. A **764**, 42 (2006).

[61] D. J. Hartley, L. L. Riedinger, R. V. F. Janssens, S. N. T. Majola, M. A. Riley, J. M. Allmond, C. W. Beausang, M. P. Carpenter, C. J. Chiara, N. Cooper, D. Curien, B. J. P. Gall, P. E. Garrett, F. G. Kondev, W. D. Kulp, T. Lauritsen, E. A. McCutchan, D. Miller, S. Miller, J. Piot *et al.*, Phys. Rev. C **95**, 014321 (2017).

[62] P. N. Usmanov, A. A. Solnyshkin, A. I. Vdovin *et al.*, Phys. At. Nucl. **77**, 1343 (2014).

[63] A. Dobrowolski, K. Mazurek, and A. Góźdź, Phys. Rev. C **97**, 024321 (2018).

[64] J. Zhao, T. Nikšić, and D. Vretenar, Phys. Rev. C **102**, 054606 (2020).

[65] P. Ring and P. Schuck, *The Nuclear Many-body Problem* (Springer-Verlag, New York, 1980).

[66] G. Lalazissis, S. Karatzikos, R. Fossion, D. P. Arteaga, A. Afanasjev, and P. Ring, Phys. Lett. B **671**, 36 (2009).

[67] P. Möller, A. J. Sierk, T. Ichikawa, and H. Sagawa, At. Data Nucl. Data Tables **109-110**, 1 (2016).

[68] K. Zhang *et al.*, At. Data Nucl. Data Tables **144**, 101488 (2022).

[69] National Nuclear Data Center, http://www.nndc.bnl.gov.